**SIRM 2015 – 11th International Conference on Vibrations in Rotating Machines,
Magdeburg, Germany, 23. – 25. February 2015**

An analysis of precise positioning scenarios of the electromechanical rotating system driven by a stepping motor

Robert Konowrocki [1], Andrzej Pochanke [2], Agnieszka Pręgowska [1], Tomasz Szolc [1]

[1] Institute of Fundamental Technological Research of the Polish Academy of Sciences, ul. A. Pawińskiego 5B, 02-106 Warsaw, Poland, tszolc@ippt.pan.pl
[2] Faculty of Electrical Engineering of the Warsaw University of Technology, Pl. Politechniki 1, 00-661 Warsaw, Poland, andrzej.pochanke@ee.pw.edu.pl

Abstract

In the paper there is investigated experimentally and theoretically electromechanical dynamic interaction between the driving stepping motor and the driven laboratory belt-transporter system imitating an operation of the robotic device in the form of working tool-carrier under translational motion. The considered object is properly equipped with measurement systems enabling us a registration of studied electrical and mechanical quantities. The analytical considerations are performed by means of the circuit model of the electric motor and of the discrete, non-linear model of the mechanical system. In the investigated examples various scenarios of the working tool-carrier motion and positioning by the belt-transporter are measured and simulated, where in the all cases the electric current control of the driving motor has been applied.

1 Introduction

The problem of dynamic interaction between several rotating systems co-operating with various electric machines, i.e. asynchronous and synchronous motors and generators as well as with DC and stepping motors, has been considered till present by many authors for many years, [1-11]. Majority of research in this field carried out using more or less advanced electromechanical models have been focused on steady-state operating conditions of the investigated objects, as e.g. in [1-5]. But the currently observed fast development of precise auxiliary drives of machines, vehicles and aircrafts as well as of robotic devices commonly driven by electric motors requires deeper and deeper knowledge about their transient operation properties. Apart of a realization of possibly precise motions, such factors as appropriately short durations of positioning times, electric power consumption and dynamic loadings imposed on the system moving elements are usually the most important from the engineering practice point of view. An interdependence of the mentioned above factors associated with the considered processes essentially follows from dynamic properties of the driven mechanical system as well as from output characteristics and control of the driving electric motor.

The stepping motors are commonly known sources of power usually applied for a possibly exact positioning of selected elements of driven precise mechanical systems. On the one hand, in such systems an accuracy of positioning essentially depends on electrical properties and proper control of the driving motor. But on the other hand, this accuracy follows from flexibility and dynamic properties of the driven object. Here, because the flexible mechanical systems usually indicate a natural ability of vibrations causing a fluctuation of the angular velocity of the stepping motor rotor, the flows of electric currents in the motor windings become affected by these mechanical oscillations, which results in additional variable components of the driving electromagnetic torque generated by the stepping motor. According to the above, the electrical current oscillations are coupled with mechanical vibrations of the driven object. In order to assure a possibly accurate positioning of elements of the mechanical systems driven by the stepping motors, the phenomenon of electromechanical interaction between the mechanical and electrical parts should be thoroughly investigated theoretically and experimentally.

This problem has been considered till present by many authors, but usually from the viewpoint of modelling of the stepping motor. Majority of them have applied the circuit models of the stepping motor and the driven mechanical system was reduced to only one rigid body, the mass moment of inertia of which is added to that of the motor rotor, as e.g. in [5-8]. In [5] one can find fundamentals of electrical modelling of the stepping motor.

The main target of investigations performed in [6-8] was a possibly the most exact control of the stepping motor operation in order to assure a precise angular positioning of the rotor. For this purpose in [6] an influence of electrical parameters of the motor and its controller has been studied. In [7,8] various stepping motor controllers were developed, where in [8] also higher harmonic components of the motor electromagnetic torque have been taken into consideration for an analysis of a possible resonance excitation. Some introductory attempts to investigations of dynamic interaction between the driving stepping motor and the driven mechanical system can be found in [9] and [11], where apart of circuit models of the electric unit the inertial-visco-elastic properties of the mechanical system have been taken into consideration respectively in the form of a structural discrete-continuous and discrete model. In [9] there was realized one of the first approach to more qualitative analysis of the circuit model of the stepping motor interacting with the torsionally vibrating structural model of the geared drive system, where all necessary geometrical and material parameters were taken into consideration. In that paper, in addition to simulation examples of transient and steady-state operating conditions, also a qualitative spectral analysis of the electrical-to-mechanical response has been performed. In [11], similarly as in [9], the voltage-frequency control of the stepping motor was applied for the theoretical electromechanical model of a robotic device.

In the paper presented here there is studied a dynamic interaction between the real two-phase hybrid stepping motor and the existing real mechanical laboratory belt-transporter system representing a robotic device characterized by the moving inertial working tool-carrier under translational motion. The main goal of this work is to develop a possibly effective and exact positioning scenario of the tool-carrier from the viewpoint of a theoretical and experimental rotational dynamic analysis of the considered object.

2 Description of the considered object and measurement systems

The real object of considerations is the above mentioned laboratory belt-transporter system imitating a robotic device characterized by the moving inertial working tool-carrier under translational motion. A photograph of this mechanism is shown in Fig. 1. The translational motion of the tool-carrier is realized by the toothed belt spanned on two rollers of the radius 0.1 m. The axes of these rollers are mutually separated by 4.375 m. The tool carrier trolley moves directly along the guideway made of the single Hepco construction beam with a nominal length of 3980 mm and a cross section of 317 mm^2. This entire structure is suspended by an aluminium truss frame which can be additionally stiffened by rigid plate elements in order to assure possibly horizontal movement of the working tool-carrier, i.e. without remarkable vertical deflections during tests. This mechanism is driven by the double-phase stepping motor FL110STH by means of the shaft segment connecting the motor rotor with the left-hand roller, see Fig.1. A schematic view of this entire object is presented in Fig. 2.

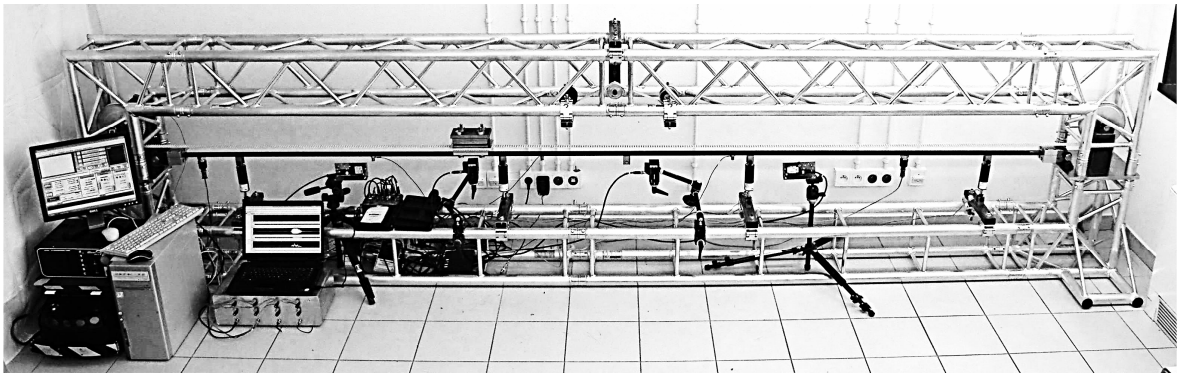

Figure 1: The laboratory belt-transporter system driven by the stepping motor.

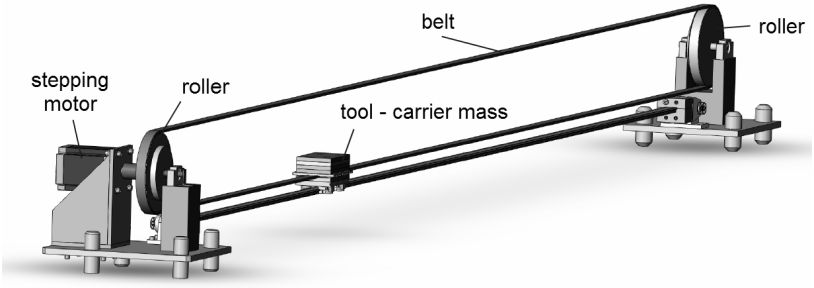

Figure 2: Scheme of the laboratory belt-transporter system driven by the stepping motor.

A rotational speed of this motor can be changed by means of the controller USN-1D8A and monitored using the rotary encoder AMT 103 mounted on the axle of the driving motor. Additionally, this encoder enables the measurement of the distance which overcomes the moving mass during testing. The tool-carrier resting on the trolley can be accelerated and decelerated during experimental tests with the rate up to of 5 m/s^2. These settings enable us to get the maximum mass velocity equal to 4 m/s. More fundamental parameters of this test-rig can be found in Table 1.

Table 1: Technical parameters of the test rig

	Parameter	**Value**
1.	maximum braking torque of the driving motor FL110STH	21 Nm
2.	maximum current of the controller USN-1D8A	7 A
3.	velocity range of the moving mass	0 - 4 m/s
4.	maximum acceleration and deceleration of the moving mass	5 m/s^2
5.	mass of the tool-carrier with the trolley	7 kg
6.	distance between the roller axles / roller radius	4.375 m / 0.1005 m
7.	maximum travel distance of the moving mass along the guideway	3.80 m
8.	resolution of the rotary encoder AMT 103	2048 p/rev
9.	sampling of the measurement card NI USB-6218 during tests	2 kS/s
10.	sensitivity of accelerometer PCB 356B18	102 mV/(m/s²)
11.	mass of the transporter belt AT10	~1.2 kg
12.	longitudinal stiffness of the transporter belt AT10	726800 N/m

A translational motion of the tool-carrier is controlled by means of the triaxial accelerometer PCB 356B18 and using the rotary capacitive encoder AMT 103. The acceleration sensor is mounted on the trolley carrying the moving tool-carrier. It measures the translational acceleration of the moving tool-carrier during tests. The measured acceleration signal is filtered by Butterworth filter. In the considered case the filter characteristic of the 5th order was used as well as the low-pass region with the 20 Hz threshold value has been selected. The frequency response of the Butterworth filter approximation function is also often referred to as 'maximally flat' response, because the applied pass-band is designed to have a frequency response which is as flat as mathematically possible in the cut-off frequency range. This filter is able to pass all frequency signals in the cut-off range, but also to attenuate signals with frequencies lower than the cut-off frequency. This is the reason, why such a filter has been applied.

During tests also variable values of electric currents in the stepping motor windings can be registered. In order to measure electric currents in both phases of the motor windings, into each of them a resistor of resistance 0.1 ohm has been connected in series. Here, the registered voltage drops across these resistors become, according to Ohm's law, the measures of current values in a given phase of the stepping motor. In the measurement system of the considered test rig presented in Fig. 1 all signals from the circuits of the stepping motor power supply, from the accelerometer and from the capacitive encoder are recorded by the analog-digital converter NI USB-6218 with the sampling frequency of 2 kS/s.

The translational velocity of the moving tool-carrier and the motor rotor rotational speed are measured by means of the capacitive encoder. A high resolution of the encoder reaching 2048 points per revolution makes it very convenient for such measurements and for recording an angular speed fluctuation of the drive system rotating elements. Upon a converting this angular speed into the translational one, the translational velocity of the moving tool-carrier can be determined. Then, by means of the time-integration of the translational velocity the distance travelled by the tool-carrier is obtained. This distance enables us to specify a precise location of the moving tool-carrier at the end of the programmed motion.

The applied laboratory belt-transporter system makes possible a precise positioning of the working tool-carrier moving with various speeds and acceleration rates. Thus, a programmed positioning procedure for the working tool-carrier can be realized by means of motions with appropriate constant average accelerations and decelerations and with piece-wise constant average translational velocities.

3 Modelling of the electromechanical system

The object of modelling is the abovementioned belt-transporter system driven by the stepping motor. This mechanism imitates a robotic device characterized by the moving inertial working tool-carrier under translational motion, a structure of which is shown in Figs. 1 and 2. A dynamic behaviour of this mechanical system can be described by the non-linear discrete model of four degrees of freedom, which is presented in Fig. 3.

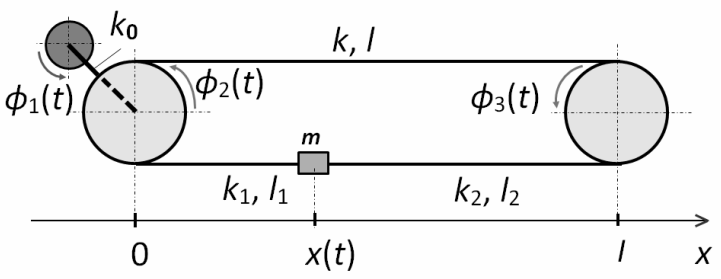

Figure 3: Physical model of the laboratory belt-transporter system.

Motion of this model is governed by the following system of ordinary differential equations:

$$
\begin{aligned}
&I_1\ddot{\varphi}_1 + d_0\dot{\varphi}_1 + c_0\left(\dot{\varphi}_1 - \dot{\varphi}_2\right) + k_0\left(\varphi_1 - \varphi_2\right) = T_{el}(t),\\
&I_2\ddot{\varphi}_2 + c_0\left(\dot{\varphi}_2 - \dot{\varphi}_1\right) + r^2c\left(\dot{\varphi}_2 - \dot{\varphi}_3\right) + rc_1(t)\left(r\dot{\varphi}_2 - \dot{x}\right) - k_0\varphi_1 + \left[k_0 + r^2\left(k + k_1(t)\right)\right]\varphi_2 -\\
&\qquad - r^2k\varphi_3 - rk_1(t)x = -\left(T_2 + F_2\dot{\varphi}_2^2\right)\mathrm{sgn}(\dot{\varphi}_2),\\
&I_3\ddot{\varphi}_3 + r^2c\left(\dot{\varphi}_3 - \dot{\varphi}_2\right) + rc_2(t)\left(r\dot{\varphi}_3 - \dot{x}\right) - r^2k\varphi_2 + r^2\left(k + k_2(t)\right)\varphi_3 - rk_2(t)x = -\left(T_3 + F_3\dot{\varphi}_3^2\right)\mathrm{sgn}(\dot{\varphi}_3),\\
&m\ddot{x} + c_1(t)\left(\dot{x} - r\dot{\varphi}_2\right) + c_2(t)\left(\dot{x} - r\dot{\varphi}_3\right) - rk_1(t)\varphi_2 - rk_2(t)\varphi_3 + \left(k_1(t) + k_2(t)\right)x = -\left(T_4 + F_4\dot{x}^2\right)\mathrm{sgn}(\dot{x}),
\end{aligned}
\tag{1}
$$

where $\varphi_i=\varphi_i(t)$, $x=x(t)$, i=1,2,3 are respectively the rotational and translational time-dependent generalized coordinates describing rigid body- and vibratory motion of the discrete mechanical model, I_1 denotes the mass moment of inertia of the stepping motor rotor, I_2, I_3 are the mass moments of inertia of the belt-transporter rollers of radius r, m is the mass of the tool-carrier, k_0, c_0 denote respectively the torsional stiffness and material damping coefficient of the shaft segment connecting the motor rotor with the driving roller, k, c are the constant and $k_1(t)$, $c_1(t)$, $k_2(t)$, $c_2(t)$ are the variable, tool-carrier position dependent longitudinal stiffness and material damping coefficient of the pre-tensiled belt between the driving and driven roller, between the driving roller and the tool-carrier and between the tool-carrier and driven roller, respectively, see Figs. 2 and 3. The symbols $T_e(t)$ and d_0 denote the electromagnetic torque function and the absolute rotor-to-stator mechanical damping coefficient. In this model there is assumed that the retarding torques and the retarding force imposed respectively on the both rollers and on the tool-carrier are expressed as sums of slowly varying components T_j representing dry friction effects in the drive system and of the square functions of the current rotational or translational speed $F_j\omega_j^2(t)$, where j=2,3,4 and $\omega_j(t)=\dot{\varphi}_j$ for j=2,3, $\omega_j(t)=\dot{x}$ for j=4 and F_j denote the proper constant coefficients.

Here, for the assumed proportional material damping in the system the constant and variable belt longitudinal stiffness and damping coefficients can be determined by means of the following formulae:

$$
c = \gamma k,\ c_i(t) = \gamma k_i(t),\ i = 1,2,\ k = \frac{EA}{l},\ k_1(t) = \frac{EA}{x(t)},\ k_2(t) = \frac{EA}{l - x(t)},
\tag{2}
$$

where EA is the belt longitudinal cross-sectional stiffness, l denotes the distance between the roller axles, see Figs. 2, 3 and Table 1, and γ is the constant material loss factor.

In the considered case of the electromechanical system governed by Eqs. (1) and according e.g. to [5,9,11], the circuit model of the two-phase hybrid stepping motor, usually characterized by the negligible fluctuation of the rotor-to-stator reluctance, can be described by two voltage ordinary differential equations of the first order:

$$
L_0\frac{di_1(t)}{dt} - \frac{d\varphi_1(t)}{dt}\left[K_U\sin\left(Z_r\varphi_1(t)\right)\right] + R\,i_1(t) = U\,\mathrm{sgn}\{\cos(\Phi(t))\},
\tag{3}
$$

$$
L_0\frac{di_2(t)}{dt} + \frac{d\varphi_1(t)}{dt}\left[K_U\cos\left(Z_r\varphi_1(t)\right)\right] + R\,i_2(t) = U\,\mathrm{sgn}\{\sin(\Phi(t))\},\qquad \Phi(\mathrm{t}) = \frac{\pi}{2}\int_0^t f_e(\tau)\,\mathrm{d}\,\tau,
$$

where $i_1(t)$, $i_2(t)$ denote the electric currents in both motor phases, L_0 is the phase inductance, R denotes the resistance of the one phase, K_U is the motor voltage constant, U is the maximal value of control voltage, Z_r denotes the rotor pole number and $f_e(t)$ is the voltage supply commutation frequency. Here, in a case of sufficiently good commutation realized by means of a proper stepping motor control, the control voltage supply phase angle $\Phi(t)$ should be followed by the motor rotor electric angle $Z_r\varphi_1(t)$. Then, the electromagnetic torque generated by such a double-phase stepping motor is expressed by the following formula:

$$T_{el}(t) = K_T\left[-i_1(t)\sin\left(Z_r\varphi_1(t)\right)+i_2(t)\cos\left(Z_r\varphi_1(t)\right)\right], \tag{4}$$

where K_T denotes the stepping motor torque constant.

4 Numerical interpretations of the electric current control of the stepping motor

In the case of the voltage-frequency control of the stepping motor applied in [9,11] Equations (1), (3) and (4) were combined together into the form of a one coupled system of ordinary differential equations describing electromechanical coupling effects between the driving electric motor and the driven mechanical system, where the variable control voltage $U(t)$ and the commutation frequency $f_e(t)$ played a role of input quantities. Since the current control of the stepping motors seems to be more convenient in an engineering practice as well as such a control concept has been applied in the considered real object, it is necessary to describe it mathematically for the aim of numerical simulations. Thus, applying the current control approach, time-histories of the electric currents $i_1(t)$ and $i_2(t)$ in the motor phases are 'a priori' assumed in the following form of harmonic functions:

$$i_1(t) = i_{\max}\cos\left(\frac{(n(t)-1)\pi}{2c}\right) \quad \text{and} \quad i_2(t) = i_{\max}\sin\left(\frac{(n(t)-1)\pi}{2c}\right), \tag{5}$$

where $i_{\max}$ is the maximal current value in the motor phases, c denotes the number of rotor micro-steps per one full step and $n(t)$ is the integer, time-dependent number of electric current feeding impulses per one micro-step. Then, by substituting (5) into (4) the electromagnetic torque $T_{el}(t)$ can be expressed in the sinusoidal form:

$$T_{el}(t) = K_T i_{\max}\sin\left(\frac{(n(t)-1)\pi}{2c} - Z_r\varphi_1(t)\right), \tag{6}$$

where the argument of the sine-function is a difference between the rotor electric angle $Z_r\varphi_1(t)$ and the 'control angle' $(n(t)\text{-}1)\pi/2c$. Here, this electromagnetic torque must always balance the sum of all inertial and passive external loadings imposed on the driven mechanical system, motion of which has been described by Eqs. (1). Moreover, in the considered case of the current control the electromagnetic torque $T_{el}(t)$ expressed by relation (6) can be regarded as an explicit external excitation source in order to obtain a system transient or steady-state dynamic response by means of a direct integration of Eqs. (1).

In this paper a proper determination of function $T_{el}(t)$ has been carried out in two alternative ways for the aim of increasing a reliability of expected theoretical results. The first way, realized by means of the original authors' computer code, reduced to determination of $n(t)$ from the equation of equilibrium between $T_{el}(t)$ described by (6) and the sum of all inertial and passive external loadings expressed by functions of accelerations and velocities corresponding to a given expected motion scenario. In the case of the second way, realized using the MATLAB-SIMULINK commercial code, $n(t)$ was determined on-line, during direct integrations of Eqs. (1), where the predictor-corrector approach has been applied for a current tracking of a correct system motion with programmed average accelerations, decelerations and constant velocities following from the assumed scenario.

5 Positioning scenarios for the belt transporter system

In the theoretical computational examples in [11] the main target reduced to positioning of the mechanical system into a given configuration within an assumed time of duration by the use of voltage-frequency control of the stepping motor. Here, because of the existing limits of admissible accelerations, maximal rotational and translational velocities and of the motor driving torque characterizing the considered real electromechanical object, see Table 1, the investigated experimentally and theoretically positioning scenarios had to be properly programmed according to boundaries of these parameters. Thus, in each studied case the mowing tool-carrier used to travel exactly the same distance 3.765 m to the given point between the rollers with various admissible rates of constant accelerations, decelerations and velocities, but with different times of duration. Such positioning scenarios have been analyzed from the viewpoint of practical efficiency, i.e. times of duration, magnitudes of mechanical vibrations and inertial loadings as well as of the consumed electric energy. Since the typical industrial controller of the applied stepping motor enabled us realizations of system motions only with constant average accelerations, decelerations and constant average velocities, the experimentally registered positioning scenarios were reduced to trapezoidal and triangular modes. This means that the tool-carrier of the

laboratory robotic device was accelerated from its standstill at the left-hand side extreme belt location, see Figs. 2 and 3, within the required time instant to the assumed constant average translational velocity and after a given time of travel duration it has been decelerated back to a standstill. Such movements were realized by means of the stepping motor current control. In Figs. 4 and 5 there are demonstrated time-histories of the measured electromechanical dynamic responses of the considered real object registered for two extremely different positioning scenarios. In Fig. 4 the results of the 'trapezoidal' mode are presented, where the tool-carrier mass has been accelerated within 0.2 s to the constant average velocity equal ~1 m/s and then upon 3.44 s decelerated to its standstill in order to overcome distance 3.765 m within 3.9 s. Figs. 4a and 4b show respectively the plots of mass velocity and acceleration. Fig. 4c presents the plot of mass travelled distance and in Fig. 4d time-histories of the control currents in both motor phases are depicted by the black and grey lines. In an identical way, in Fig. 5 there are shown analogous measured results registered for the 'triangular' positioning mode, where the tool-carrier mass was accelerated within 0.86 s to the maximal admissible speed ~4 m/s and then immediately decelerated to its standstill. Here, the travelled distance 3.765 m has been overcome within 1.76 s only. However, Figs. 6 and 7 present analogous time-histories of respectively the same quantities determined by means of numerical simulations for the identical as above positioning scenarios. The black lines in Figs. 6a,b,c and 7a,b,c correspond to the results obtained by means of the mentioned above current control approach implemented in the authors' original computer code and the plots denoted by the grey lines correspond to the results determined using the current control strategy realized by the program operating in the framework MATLAB-SIMULINK software package. These theoretical results have been obtained for the abovementioned parameters of the real mechanical system listed in Section 2 and in Table 1 as well as for parameters of the applied hybrid, four-cycle, double-phase stepping motor FL110STH characterized by L_0=15 mH, R=0.8 Ω, K_T =2.2845 Nm/A and by the fundamental step angle 1.8 deg=0.0314 rad, which means that its rotor has Z_r=50 poles. The current control of the motor operation was realized for i_{max}=7 A and for the commonly used c =8 rotor micro-steps per one full step. The mass moment of inertia of the toothed belt has been uniformly reduced to the axes of both rollers.

It is to emphasize that a very good qualitative and quantitative agreement between the corresponding experimental and theoretical results have been obtained, particularly using the authors' original computer code. Here, the registered mutual discrepancies between the theoretical results obtained using the two mentioned above simulation approaches occur mainly for oscillation local amplitude values. These differences are caused by a

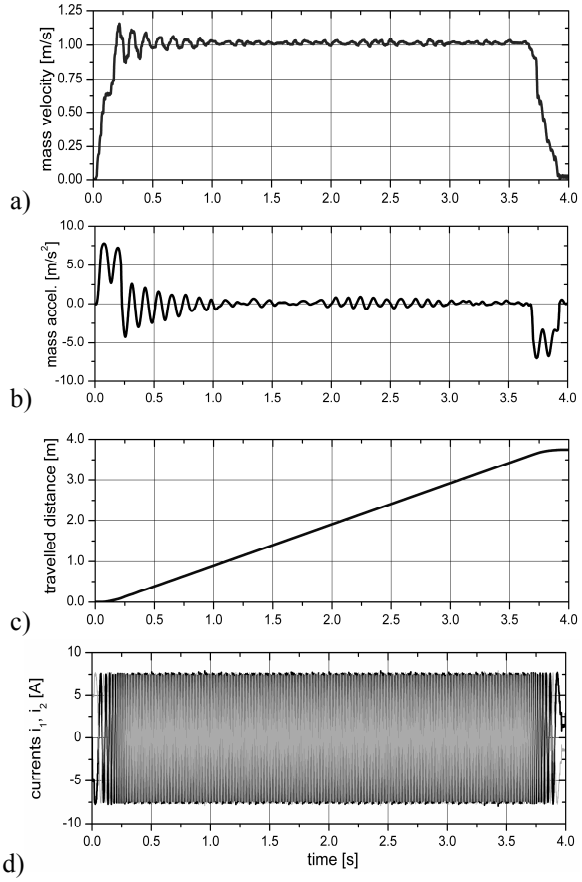

Figure 4: Measured system response for the 'trapezoidal' positioning mode with v_{max}=1 m/s.

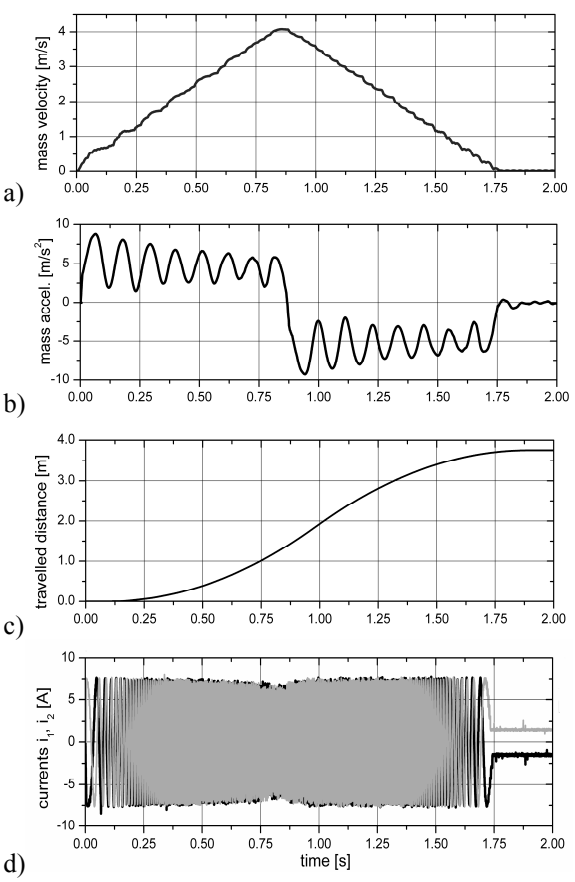

Figure 5: Measured system response for the 'triangular' positioning mode with v_{max}=4 m/s.

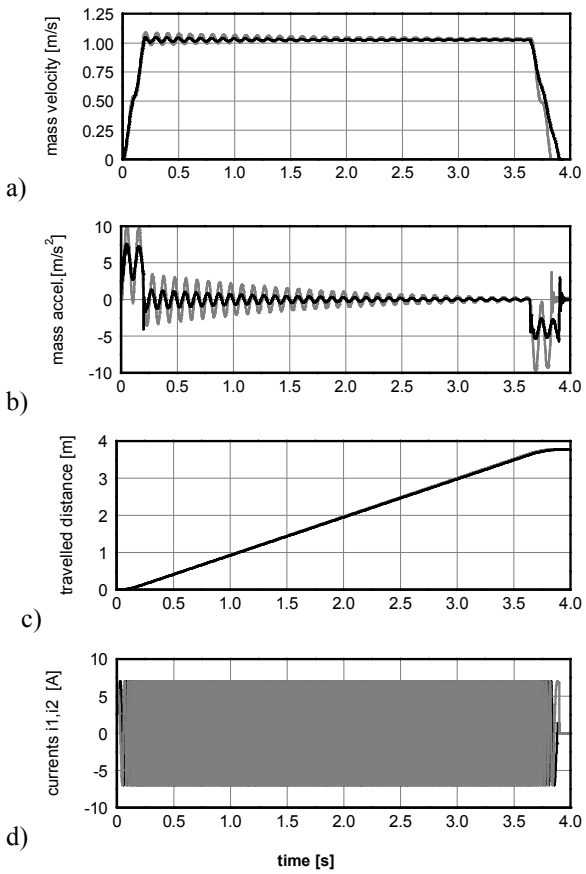

Figure 6: Simulated system response for the 'trapezoidal' positioning mode with v_{max}=1 m/s.

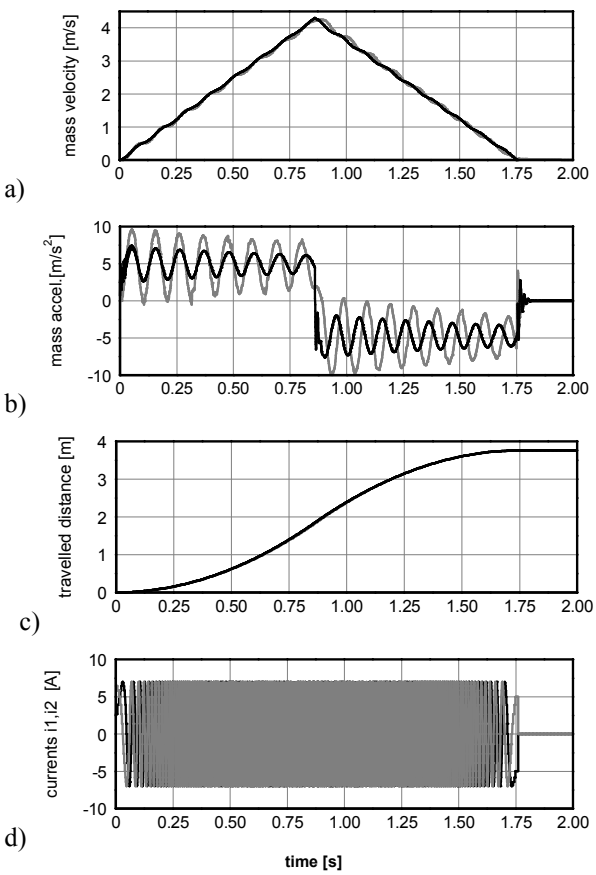

Figure 7: Simulated system response for the 'triangular' positioning mode with v_{max}=4 m/s.

some kind of 'numerical inertia' observed during the on-line tracking of the assumed motion scenarios realized by the MATLAB-SIMULINK commercial code, regardless applied lengths of the direct integration steps. Furthermore, for the aim of a better explanation of properties of the all measured results, in Figs. 8 and 9 there are shown time-histories of the simulated electromagnetic torques generated by the stepping motor together with plots of the system resultant external retarding torques reduced to the motor rotor axis and with the dynamic torques transmitted by the shaft segment connecting the motor-rotor with the left-hand roller, see Figs. 2 and 3. Here, Fig. 8 corresponds to the abovementioned 'trapezoidal' positioning scenario and Fig. 9 to the 'triangular' one. In these figures by the grey solid lines the electromagnetic torque time-histories are plotted, by the black lines there are depicted the time-histories of the shaft visco-elastic dynamic torques and the black dashed correspond to the retarding torques. In the both cases of the positioning scenarios, i.e. the 'trapezoidal' and the 'triangular' one, the time-histories of the electromagnetic motor torque are characterized by the low- and high-frequency fluctuating components. The latter of rather steady-state oscillation amplitudes is caused by the step-wise, discontinuous character of a commutation realized by the current control with the given number c of micro-steps per one full step. From some auxiliary numerical simulations carried out for various c equal to 16, 32 and 64 it follows that if the number of micro-steps increases, amplitudes of the electromagnetic torque high-frequency component tend to zero. In a contradistinction, the low-frequency motor torque component gradually decays with time. But these transient oscillations of relatively greater amplitudes very significantly influence also time-histories of the tool-carrier accelerations and velocities, which has been confirmed by experimental measurements for the both considered positioning scenarios, as shown in Figs. 4a,b and 5a,b.

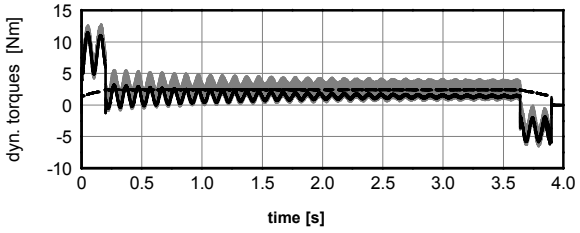

Figure 8: Simulated dynamic torques for the 'trapezoidal' positioning mode with v_{max}=1 m/s.

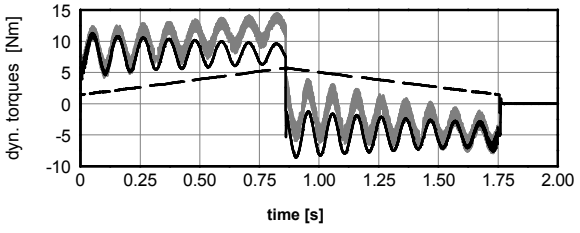

Figure 9: Simulated dynamic torques for the 'triangular' positioning mode with v_{max}=4 m/s.

These low-frequency transient vibrations induced after each rapid change of the programmed average acceleration in the framework of the realized positioning scenario are caused by the dynamic interaction between the electric motor and the driven mechanical system. Here, similarly as in the case of induction motors investigated in [4] and [10], the studied 'free-free' torsional train presented in Figs. 2 and 3 becomes rotationally clamped by the stepping motor stator. According to [5], the rotational stiffness of the electromagnetic spring connecting the motor rotor with the stator can be expressed as $k_e=Z_r \cdot K_T \cdot i_{\max}$., where the symbols standing on the right-hand side have been already defined in Eqs. (3), (4) and (5). Then, upon eigenfrequency analyses performed for the undamped and linearized mechanical system, i.e. for the assumed stationary positions of the tool-carrier $x_1=r$, $x_2=l/2$ and $x_3=l$-r, see Fig. 3, and for the additional 'clamping' elastic term $k_e\varphi_1(t)$ standing on the left-hand side of Eq. $(1)_1$ the first natural frequency values are equal to 10.14 Hz for x_1, 9.89 Hz for x_2 and 9.74 Hz for position x_3, where the natural frequencies corresponding to higher eigenmodes exceed 60 Hz. This result fits well to all respective time histories presented in Figs. 4a,b, 5a,b, 6a,b, 7a,b as well as in Figs. 8 and 9.

From a qualitative comparison of the both considered scenarios it follows that the 'triangular' one lasts more than two times shorter, but it requires system acceleration to 4 times greater maximal velocity than the 'triangular' mode, which results in more severe transient low-frequency oscillations. Nevertheless, in the both cases the amplitudes of tool-carrier deceleration at the end of movement, i.e. during the final positioning, are similar to each other, which results in comparable peak values of the inertial forces associated with braking of the moving tool-carrier. These properties have been experimentally and theoretically confirmed by the third, also 'trapezoidal' positioning scenario, where the tool-carrier was accelerated to the maximal average constant velocity ~2 m/s within 0.44 s and upon 1.44 s decelerated back to a standstill within next 0.41 s. Thus, the entire positioning process lasted 2.29 s, which is essentially shorter than in the case of the previous 'trapezoidal' mode and only 0.53 s longer than the 'triangular' one. The time-history plots of the of the tool-carrier velocity, acceleration, travelled distance and of the control currents, which were measured and simulated using the both methods mentioned in Section 4, are presented in Figs. 10 and 11 in an identical way as in Figs. 4, 5, 6 and 7.

From an analysis of the experimentally and theoretically obtained pots it follows that this positioning scenario is characterized by similar qualitative and quantitative properties as those two considered above. First of all, after each rapid change of the average acceleration also the severe transient oscillations of frequency ca. 10 Hz are induced. Moreover, despite of only two times greater average maximal velocity than in the case of

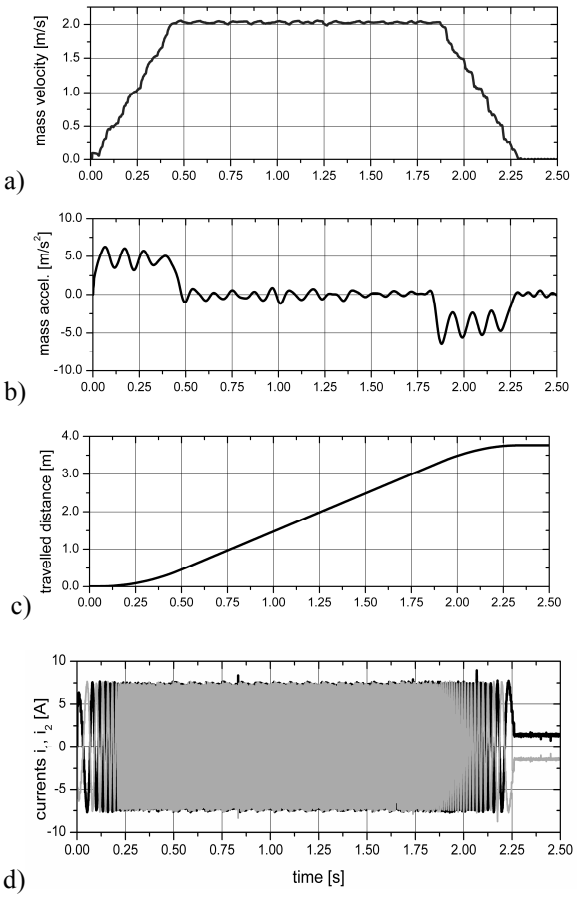

Figure 10: Measured system response for the 'trapezoidal' positioning mode with $v_{\max}$=2 m/s.

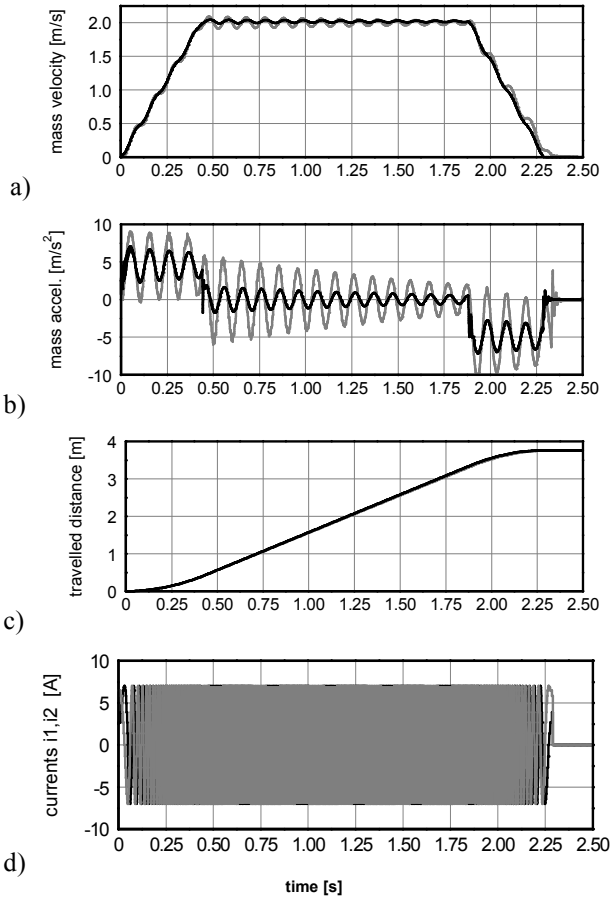

Figure 11: Simulated system response for the 'trapezoidal' positioning mode with $v_{\max}$=2 m/s.

previous 'trapezoidal' mode the entire mechanical system must have been braked to a standstill with a comparable average deceleration as those realized before. Namely, the deceleration values necessary for braking the moving tool-carrier were equal to ~3.85 m/s^2 in the case of 'trapezoidal' mode with v_{max}=1 m/s, ~4.88 m/s^2 for the 'trapezoidal' mode with v_{max}=2 m/s and ~4.44 m/s^2 in the case of 'triangular' mode. This means that during realizations of all these three positioning scenarios comparably high inertial forces act on the braked tool-carrier, which can negatively influence a precision of its motion. Thus, in order to avoid disadvantages of these all positioning scenarios considered above and to achieve a possibly short time of tool-carrier motion within the admissible speed range 0-4 m/s, see Table 1, the applied till present step-wise, rapid changes of the system average accelerations can be modified by an alternative fluent one characterized by a sinusoidal form which results in a cosinusoidal variation of the tool-carrier average velocity. Since the stepping motor controller applied here enables us to realize motions only with constant average accelerations and velocities, such proposed 'cosinusoidal' positioning scenario has to be investigated theoretically. In Fig. 12 there are shown corresponding results of simulation for the tool-carrier overcoming the same travelled distance 3.765 m within 1.76 s and with v_{max}=4 m/s, i.e. for identical parameters as in the case of the 'triangular' mode. Using the black lines Figs. 12a,b and 12c present time-histories of the tool-carrier velocity, acceleration and travelled distance, respectively. For a comparison, in these figures by means of the grey lines also the analogous time-histories corresponding to the considered above 'triangular' mode are plotted. In an identical way as in Figs. 8 and 9, for the 'cosinusoidal' positioning scenario there are depicted time-histories of the stepping motor electromagnetic torque (grey line) together with time-histories of the dynamic torque transmitted by the shaft segment connecting the motor-rotor with the left-hand roller (black solid line) and of the resultant external retarding torque acting on the entire mechanical system (black dashed line). For the aim of a better demonstration of differences between the all four considered positioning scenarios as well as of emphasizing advantages of the proposed 'cosinusoidal' mode, in Figs. 12e and 12f in the travelled distance domain there are respectively presented plots of the tool-carrier movement trajectories and of the braking force histories. In these figures the black solid lines correspond to the 'cosinusoidal' positioning scenario, the grey lines to the 'triangular' one and using the dotted and dashed lines the plots corresponding to the 'trapezoidal' modes with respectively v_{max}=1 m/s and v_{max}=2 m/s are depicted.

From an analysis of successive plots in Figs. 12a-f there follow several advantages of the 'cosinusoidal' positioning scenario in a comparison with the 'triangular' and both 'trapezoidal' ones. First of all, the fluent, 'jump-free' variation of the average movement acceleration results in significantly smaller amplitudes of the low-frequency transient vibrations, as shown in Figs. 12a,b. Moreover, the total time of tool-carrier run can be here as short as in the case of the 'fastest' 'triangular' mode. Although the 'cosinusoidal' positioning scenario is realized with instantaneously the greatest average accelerations and velocities of the moving tool-carrier and of all system rotating parts, see Figs. 12a,b,e, but their motions are forced by the electromagnetic and dynamic torques characterized by smaller oscillation amplitudes and much more fluent variation in time, as indicated in Fig. 12d, in a comparison with the analogous plots in Figs. 8 and 9. This feature seems to be very convenient from the viewpoint of material fatigue, unnecessary noise generation and heat losses. But the greatest benefits

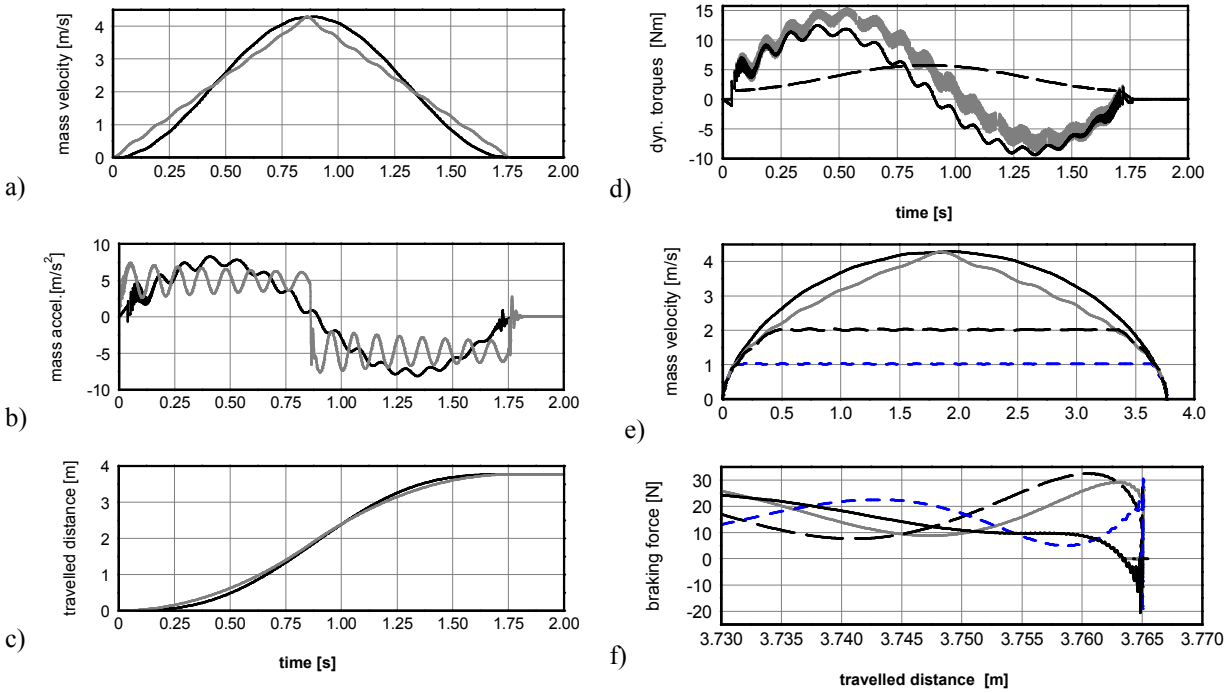

Figure 12: Simulated system response for the 'cosinusodal' positioning mode with v_{max}=4 m/s.

associated with an application of the proposed 'cosinusoidal' scenario seem to follow from the smallest braking forces occurring at the time instant of tool-carrier positioning at the target distance 3.765 m. The respective plots in Fig. 12f indicate remarkably the mildest braking force fluctuation observed in this case, which creates the best conditions for possibly precise placements of mechanical system elements to the given point. Nevertheless, the instantaneous bigger average accelerations and velocities associated with the 'cosinusoidal' scenario result in the highest electric energy consumption due to appropriately greater retarding forces and torques. The consumed electric energies calculated using Eqs. (3) for the 'trapezoidal' modes with v_{max}=1 and v_{max}=2 m/s as well as for the 'triangular' and 'cosinusoidal' ones were respectively equal to 90.16, 122.64, 160.28 and 174.06 Ws.

5 Final remarks

In the paper there was performed an experimental and theoretical investigation of an operation of a real electromechanical system in the form of the laboratory robotic tool-carrier moved by the belt-transporter system driven by the stepping motor. By means of this device several scenarios of the tool-carrier positioning were analyzed using results of measurements and numerical simulations, for which a very good mutual qualitative and quantitative agreement has been obtained. These scenarios consisted of system movements characterized by piece-wisely constant as well as continuously variable average accelerations and velocities. It turned out that rapid changes of these average accelerations and velocities resulted in excitation of severe low-frequency transient torsional and translational vibrations induced by the electromechanical interaction between the driving motor and the driven system. Moreover, these oscillations superimposed on the nominal motions with high constant average deceleration rates during tool-carrier positioning to the target point were associated with relatively large braking force fluctuations negatively influencing a precise operation of the considered device. However, tool-carrier positioning scenarios characterized by fluent, continuous variations of system average accelerations, decelerations and velocities resulted in essentially smaller transient low-frequency vibrations and in significantly lower amplitudes of braking forces. Thus, such movement scenarios seem to be particularly promising for programmed precise operations of numerous responsible electromechanical devices.

Acknowledgement

The investigations supported by the National Science Center: Research Project: UMO-2011/03/N/ST8/03904.

References

[1] Tabesh, A. and Iravani, R. (2005): On the application of the complex torque coefficients method to the analysis of torsional dynamics. *IEEE Transactions on Energy Conversion*, Vol. 20, No. 2, pp. 268-275.

[2] Repo, A.-K., Rasilo, P. and Arkkio, A. (2008): Dynamic electromagnetic torque model and parameter estimation for a deep-bar induction machine. *Electric Power Applications*, IET, 2, 3, pp. 183-192.

[3] Xu, K., Zhao, C., Zhang, J. and Guo, C. (2011): The application of complex torque coefficient method in multi-generator system. *Electrical Power Systems and Computers*, LNEE 99, X. Wan (Ed.), Springer-Verlag Berlin Heidelberg, pp. 299-306.

[4] Szolc, T., Konowrocki, R., Michajłow, M. and Pręgowska, A. (2014): An investigation of the dynamic electromechanical coupling effects in machine drive systems driven by asynchronous motors. *Mechanical Systems and Signal Processing*, 49, pp. 118–134.

[5] Sochocki, R. (1996): *Electrical Micro-machines.* Eds. of the Warsaw University of Technology, Warsaw, ISBN 83-86569-84-0 (*in Polish*).

[6] Liu, X. and Zhao, D. (2011): The simulation of stepping motor under two kinds of condition. *Procedia Engineering* 23, pp. 464 – 467.

[7] Jahani, R., Chahkandi Nejad, H., Shayanfar, H.A. and Zare, A. (2010): Positioning control of PM stepper motor based on type-2 fuzzy robust control. *International Journal on "Technical and Physical Problems of Engineering"*, Issue 5 Vol. 2, No. 4, pp. 19-26.

[8] Wang-Hay Tsui, K., Chow Cheung, N. and Chi-Wah Yuen, K. (2009): Novel modeling and damping technique for hybrid stepper motor. *IEEE Trans. on Industrial Electronics*, Vol. 56, No. 1, pp. 202-211.

[9] Szolc, T. and Pochanke, A. (2012): Dynamic investigations of electromechanical coupling effects in the mechanism driven by the stepping motor. *J. of Theoretical and Applied Mechanics*, 50, 2, pp. 653-673.

[10] Szolc, T., Michajłow, M. and Konowrocki, R. (2013): On electromechanical dynamic coupling effects in the semi-actively controlled rotating machine drive system driven by the induction motor. In Proc. 10th Int. Conf. on Vibrations in Rotating Machines – SIRM 2013, Berlin, 25–27 February, Paper ID-258.

[11] Pręgowska, A., Szolc, T., Pochanke, A. and Konowrocki, R. (2014): Modeling and dynamic analysis of the precise electromechanical systems driven by the stepping motors. *Advances in Intelligent Systems and Computing*, Springer International Publishing Switzerland, Vol. 267, pp. 205–215.